



Trans. Nonferrous Met. Soc. China 27(2017) 2104-2111

Transactions of Nonferrous Metals Society of China

www.tnmsc.cn



Nucleation interface of Al-Sb alloys on single crystal Al₂O₃ substrate

Lu WANG^{1,2}, Lin YANG², Di ZHANG¹, Ming-xu XIA¹, Yun WANG³, Bin CHEN¹, Jian-guo LI¹

- 1. School of Materials Science and Engineering, Shanghai Jiao Tong University, Shanghai 200240, China;
 - 2. School of Materials and Engineering, Jiangsu University of Technology, Changzhou 213001, China; 3. BCAST, Brunel University, Uxbridge, Middlesex UB8 3PH, UK

Received 4 June 2016; accepted 4 January 2017

Abstract: Lattice structure information of heterogeneous nucleation at nucleation interface was present. The crystal orientation, and interfacial structure characteristic of liquid Al alloys nucleated on the basal surface (0001) Al_2O_3 single crystal substrate were identified by X-ray diffraction (XRD), scanning electron microscopy (SEM) and high resolution transmission electron microscopy (HRTEM) analysis. The preferred crystal orientations of pure Al and Al-1%Sb (mass fraction) alloy adjacent to the nucleation interface were examined as (200) and (220) planes of Al, respectively, and two corresponding orientation relationships were obtained. An improved nucleation efficiency and refined grains were attributed to both the reduced interplanar spacing of preferred orientation and the decrease of lattice misfit from 16.4% to 7.0% in $Al-1\%Sb/Al_2O_3$ nucleation group.

Key words: aluminium alloy; nucleation; interfacial structure; orientation relationship

1 Introduction

Since the first undercooling measurement executed by FAHRENHEIT [1] on the solidification of supercooled water providing the evidence for nucleation barrier, the nucleation of liquid towards a more condensed state attracts extensive scientific interests and technological attentions due to the intimate relationship with initial structure, the size scale of the structure and spatial distribution [2]. It is common practice to introduce nucleating agents during the casting process in order to reduce cast defects, form fine and uniform grains and therefore improve casting quality.

The investigation of ordering phenomena at solid-liquid interface has been carried out by various theoretical and experimental approaches [3–6] from the last century. High resolution transmission electron microscopy (HRTEM) [7,8] enables direct imaging of various interfaces at the atomistic level. For an extensive review on the epitaxy growth of general film in Ref. [9], the experimental evidence of heterostructures was presented across various misfit scales. A good lattice matching at the interface and a small undercooling

represent a potent nucleation potency of the nucleating substrate in Al/Al₂O₃ system [10]. While in aspect of grain refining, apart from nucleating agents such as Al-Ti-B in Al alloy and Al-Ti-C in Mg alloy [11-13], trace alloying element, RE, K, Na, Ca, Sr, Ba, Sn, Sb, Bi, P is also added into alloys as microstructure modifier [14-19]. In these elements, Sb is a surface-active element extensively used in Al-Si alloys, Mg-Al-Si alloys and Al-based composites [20-24], to modify eutectic structure forming at relatively high cooling rates for enhanced casting properties. There are a few works on the modification mechanism of Sb to Si, Mg₂Si phases and so on. For example, REN et al [20] presented that the nucleation site of Mg₂Si in Mg-Al-Si alloy, is enriched in Si, Mg and Sb. WANG et al [22] suggested that the coherent precipitation of AlSb can introduce stress into Si crystal forming little defects, which hinders the growth of Si. They further pointed out that Sb and Ba will enhance the modification effect of RE. To date, different modification mechanisms of Sb in Al-Si and Al-Mg-Si alloys have been achieved. However, there is very little information regarding the interface structure formed during both nucleation and solidification processes of common metal casting on the specific

Foundation item: Project (51474148) supported by the National Natural Science Foundation of China; Project (14140711000) supported by Shanghai International Cooperation Program, China; Project (U1660203) supported by Joint Funds of the National Natural Science Foundation of China

Corresponding author: Ming-xu XIA; Tel: +86-21-54744246; E-mail: mingxu.xia@sjtu.edu.cn DOI: 10.1016/S1003-6326(17)60236-X

substrates, such as the usually existed oxide Al₂O₃ in Al alloy. Correspondingly, the nucleation efficiency and refinement effect of Sb element on the heterogeneous nucleation of Al hasn't been investigated thoroughly yet.

This work aims at providing specific experimental results on nucleation behaviour of liquid Al–Sb alloy on a single crystal sapphire substrate and interfacial structure inspired by the nucleation is also investigated. The identity of nucleation interfacial structure is verified by multi-analytical technologies. Following that, the orientation relationships between the nucleation phase and substrate are experimentally determined through HRTEM. The enhanced nucleation efficiency and refining effect of Al–Sb alloy is hereupon evaluated from the crystallographic point of view, using a modified lattice matching model [25].

2 Experimental

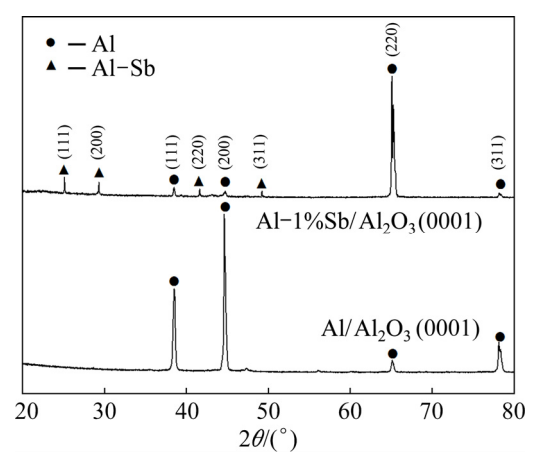
A sapphire with basal surface (0001) was used for the nucleation substrate in this work. The surface roughness of the substrate was less than 5 nm. High purity Al (99.999%, mass fraction) was purified using glass fluxing method to remove potential heterogeneous nuclei from liquid Al. To examine alloying element effect on the nucleation behavior of liquid Al and the structure configuration of nucleation interface, Sb (99.999%, mass fraction) was added into liquid Al after purification. The mass fraction of 1% was selected to ensure primary α -Al phase nucleated under an uninterfered environment, to avoid any interfere from the potential compounds, according to Al-Sb phase diagram [26]. Al-1%Sb (mass fraction) alloy was prepared by arc melting under an argon atmosphere, and then directly cast into cylindrical rods with 3 mm in diameter using a suction casting facility.

The Al₂O₃ substrate was firstly cleaned in acetone for 3 min with an ultrasonic cleanser and then placed on a gas cooling platform in a high vacuum chamber (the pressure was 2×10⁻⁴ Pa). Aluminum and its alloy samples were placed on such an Al₂O₃ substrate and then Al/Al₂O₃, Al-1%Sb/Al₂O₃ couples were heated up to 1300 K (1027 °C) by a laser beam with a heating rate of 20 °C/s. The sample was held at that temperature for 3 min before the laser beam was switched off, and then cooled down at a controlled cooling rate of 20 °C/s under a flowing argon atmosphere. The details can be referred to Ref. [27]. X-ray diffraction (XRD) analysis was employed to detect the crystal orientation of newly formed crystal from the bottom of the sample where nucleation was triggered by the substrate. Scanning electron microscopy (SEM) samples were obtained through conventional metallurgical sample preparation procedure for microstructural analysis. SEM was executed with backscattered electron (BSE) mode by Phenom XL System coupled with energy dispersive X-ray spectroscopy (EDS) analysis. Interfacial structure investigations were carried out by transmission electron microscopy (TEM) and HRTEM using a Tecnai G² F20 S-twin TEM instrument. The samples were prepared from cutting slices perpendicular to the interface with a thickness less than 80 μm before ion beam thinned using a Gatan PIPS II precision ion polishing system at 5.0 kV and an incident angle of 4°-6°.

3 Results and discussion

3.1 Crystal orientation of nucleated phase

The crystal orientation of Al alloy adjacent to the nucleation interface was examined on Al/Al₂O₃(0001) and Al-1%Sb/Al₂O₃(0001) systems using XRD analysis, as shown in Fig. 1. The result shows that the preferred crystal orientation of pure Al was (200). When Sb was added into Al liquid, the preferred crystal orientation of newly formed crystals was changed into (220). Besides the crystals of Al matrix, the AlSb compound was also detected with the (111), (200), (220) and (311) diffraction peaks. It is obvious that the crystal orientation of new crystals nucleated on the (0001) Al₂O₃ substrate was affected by the addition of Sb.



 $\label{eq:Fig. 1} \textbf{Fig. 1} \ \text{Crystal orientation of newly formed crystals adjacent to interface} \quad \text{in} \quad Al/Al_2O_3(0001) \quad \text{and} \quad Al-1\%Sb/Al_2O_3(0001) \\ \text{systems}$

3.2 Interface characteristics

SEM images at crystal–substrate interfaces of Al/Al₂O₃(0001) and Al–1%Sb/Al₂O₃(0001) systems are presented in Fig. 2. It is seen that both the interfaces between crystal phases and Al₂O₃ substrate were straight and distinct. Two phases appeared in the Al–1%Sb crystals in Fig. 2(b) compared with only one phase in counterpart Al/Al₂O₃(0001) system in Fig. 2(a). The darker and brighter phases marked as "1" and "2" in Fig. 2(b), were confirmed as matrix Al and Al–Sb

compound, respectively. While in Fig. 2(a), the phase was detected as Al. The compound in Fig. 2(b) formed either at the interface or in the matrix, both with thickness less than 5 µm. The composition of the matrix, compound and substrate was qualitatively analyzed, as shown in Figs. 3(a)–(c) as Al, Al–Sb phase and Al–O phase.

3.3 TEM and HRTEM analysis

The interfacial structure between Al and Al_2O_3 substrate has been systematically studied using TEM and HRTEM methods. Figure 4(a) shows a typical cross-sectional TEM bright-field image of $Al/Al_2O_3(0001)$ interface. A sharp and straight interface split new crystal from lower substrate. Through selected area electron diffraction (SAED) examination, it was confirmed that the upper area corresponds to Al phase, while the below substrate is Al_2O_3 .

Figure 4(b) displays a HRTEM image of Al/Al₂O₃(0001) taken along Al₂O₃ [$\overline{1}100$] axis. The interplanar spacing in the upper area was consistent with the face-centred cubic structure of Al with spacings of 2.0296 and 2.0190 Å both close to $a_{Al}/2$, while spacing in

the lower area was in accord with the hexagonal structure of Al_2O_3 with spacings of 2.3810 Å and 4.3553 Å, which are close to $a_8/2$ and $c_8/3$. The subscript "S" represents Al_2O_3 substrate. They respectively corresponded to planes $\{200\}$ of Al in upper area and $\{11\overline{2}0\}$ and $\{0003\}$ of Al_2O_3 in lower area. Among them, $(\overline{2}00)_{Al}$ and $(000\overline{3})_S$ were labelled in Fig. 4(b). It is noting that $(000\overline{3})$ plane of Al_2O_3 is perfectly parallel to the interface and meanwhile the lattice arrangement of $(000\overline{3})$ is identical to that of (0001). Therefore, the (0001) plane of Al_2O_3 is parallel to the interface. In addition, the incident beam was also aligned with $[001]_{Al}$ direction. According to the presented lattice image in Fig. 4(b), $(\overline{2}00)_{Al}$ is approximately parallel to $(000\overline{3})_S$, with a small tilt angle.

The fast Fourier transformation (FFT) image is shown in Fig. 4(c) by making Fourier transform of the HRTEM. It is seen that there are two sets of diffraction spots, one set from Al₂O₃ and the other from Al. An orientation relationship (OR) between Al and Al₂O₃ can be obtained from the diffraction pattern. A schematic index of the pattern is shown in Fig. 4(d). With the help

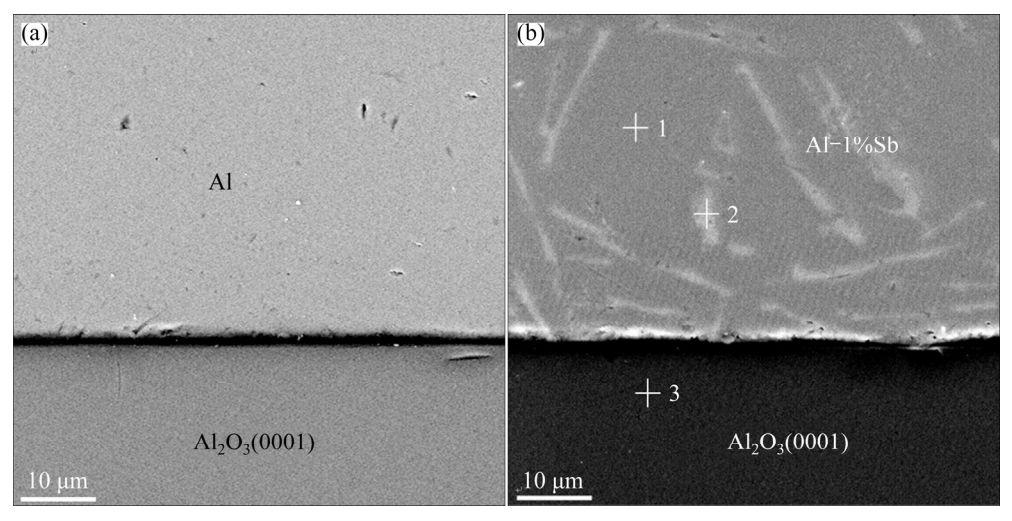


Fig. 2 SEM images of Al/Al $_2$ O $_3$ (0001) (a) and Al $_2$ O $_3$ (0001) (b) interfaces

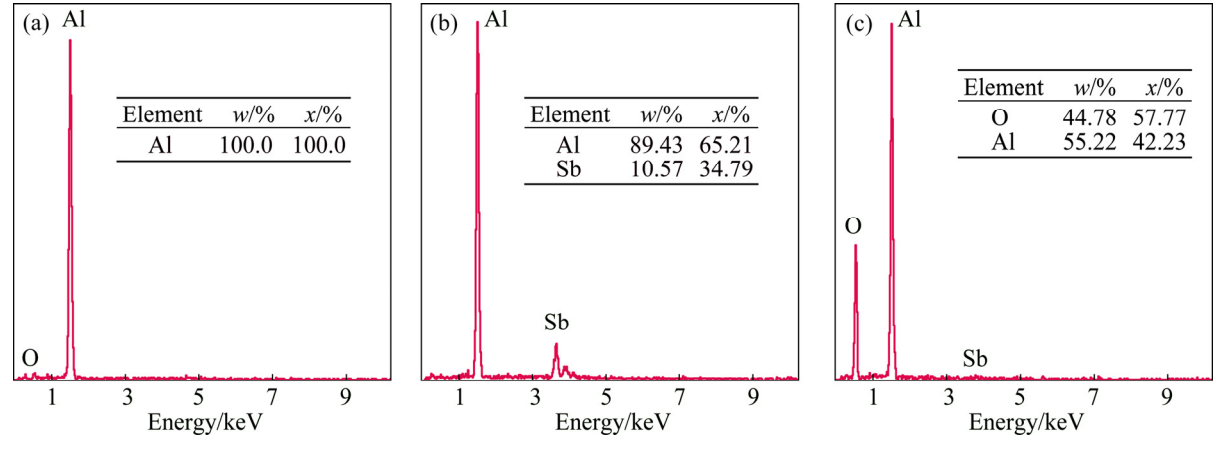


Fig. 3 EDS analysis results for matrix (a), compound (b) and substrate (c) as marked with "1"-"3" in Fig. 2(b)

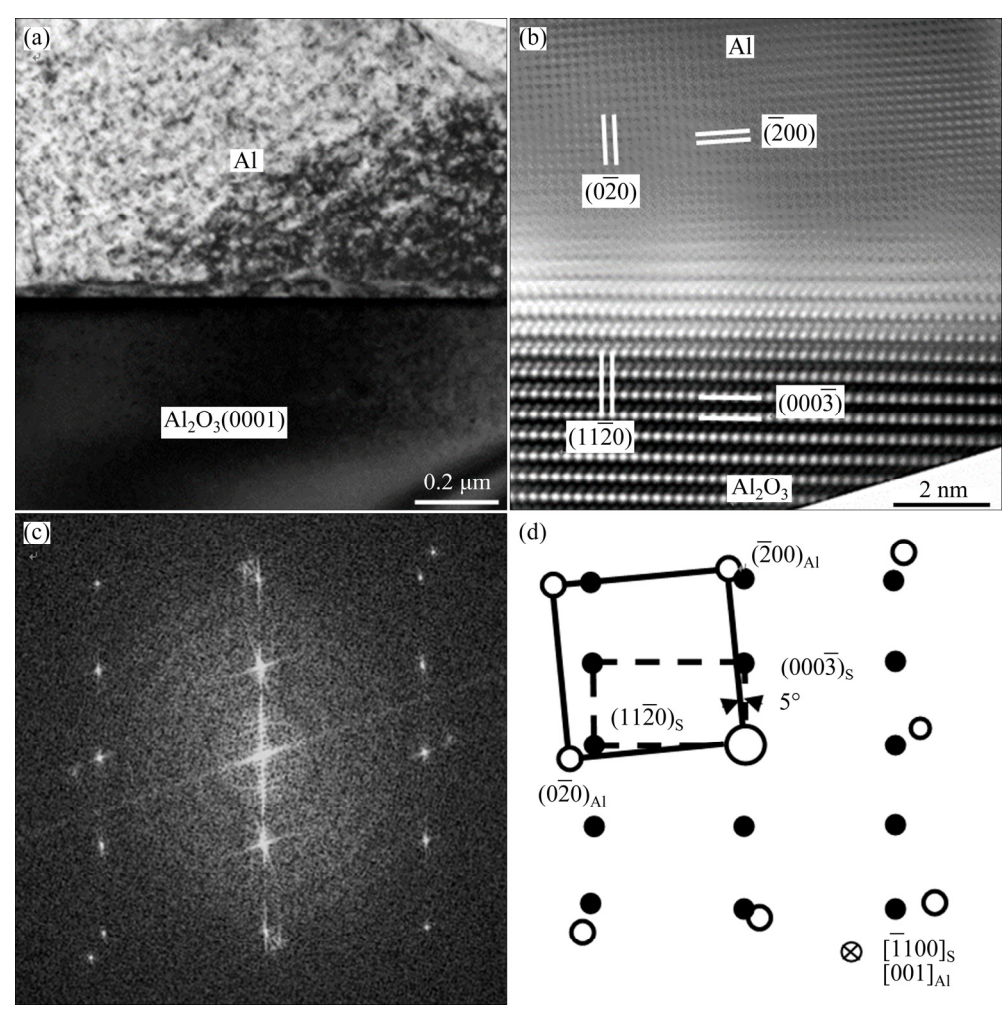


Fig. 4 Typical cross-sectional TEM bright-field image of Al/Al₂O₃(0001) interface (a), HRTEM of Al/Al₂O₃(0001) taken along Al₂O₃ $[\overline{1}100]$ axis (b), fast Fourier transformation (FFT) image of HRTEM (c), and schematic index of FFT pattern along $[\overline{1}100]_S$ and $[001]_{Al}$ zone axes, where open and filled circles represent Al and Al₂O₃ respectively (d)

of FFT pattern, a 5° tilting between the pair of parallel planes is determined. This 5° tilt is clearly seen in Fig. 4(c) and (d) by the small misorientation between diffraction spots $(000\overline{3})_S$ and $(\overline{2}00)_{Al}$. Therefore, an OR between Al_2O_3 and Al is established: $(000\overline{3})_S$ $[\overline{1}100]_S \sim //(\overline{2}00)_{Al}[001]_{Al}$.

Figure 5(a) shows a typical cross-sectional TEM bright-field image of Al–1%Sb/Al₂O₃(0001) interface. A small particle with thickness about 300 nm was observed at the interface. The up and lower areas were confirmed as Al phase and Al₂O₃ substrate through SAED analysis in Fig. 5(b). The SAED pattern was taken from the area including substrate, small particle and Al matrix across the interface viewed along $[\bar{1}100]_S$ zone axis, which exhibits three clear sets of diffraction spots. Two sets with similar interplanar spacing appear periodically and the third set with the smallest interplanar spacing has only one group of symmetrical spots. A schematic index of the pattern is shown in Fig. 5(c).

The interplanar spacing of innermost spots, the

filled circles, corresponded to hexagonal structure of Al₂O₃ with spacings of 2.3810 Å and 4.3553 Å, which are close to $a_S/2$ and $c_S/3$, $\{11\overline{2}0\}$ and $\{0003\}$ planes of Al₂O₃. The interplanar spacing for the set of outermost spots, the large open circles, was equal to the face-centred cubic structure of Al with spacings of 1.4180 and 1.2240 Å, which are close to $a_{AI}/2\sqrt{2}$ and $a_{\rm Al}/\sqrt{11}$, {220} and {311} planes of Al matrix. It is indicated that the Al crystal is orientated along [114]_{Al} zone axis. The middle set of spots was very close to the set of Al₂O₃, where the interplanar spacings are 3.5294 and 2.1490 Å for the two nearest spots from center spot. According to the XRD pattern in Fig. 1 and EDS result in Fig. 2, the small particle could be AlSb compound. AlSb is cubic ZnS structure with the lattice constant of 6.13 Å [26]. The two nearest spots could be {111} and {220} planes of AlSb, with its incident beam aligned along [112]_{AlSb} zone axis. The corresponding planes of diffraction spots were labelled in Fig. 5(c). Given (0001)_S parallel to the interface and the SAED pattern

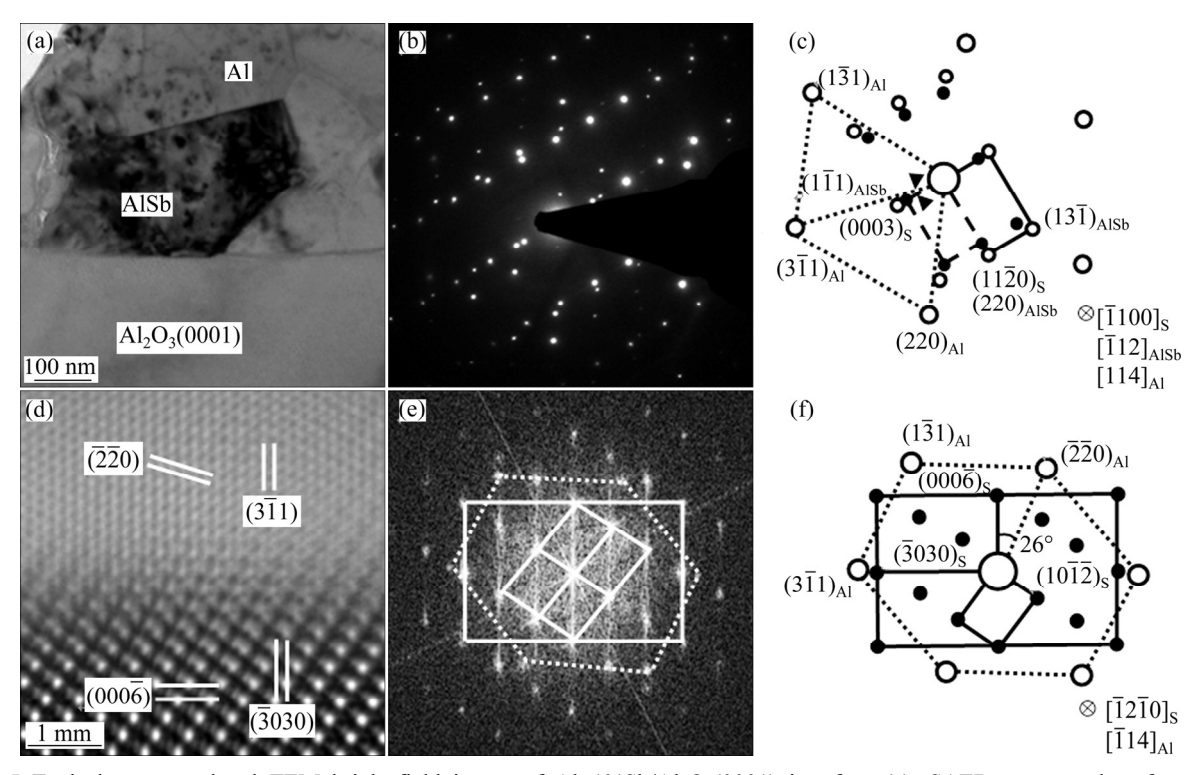


Fig. 5 Typical cross-sectional TEM bright-field image of Al-1%Sb/Al₂O₃(0001) interface (a), SAED pattern taken from area including substrate, compound particle AlSb and Al matrix across interface taken along $[\bar{1}100]_S$ zone axis (b), schematic index of SAED pattern along $[\bar{1}100]_S$, $[\bar{1}12]_{AlSb}$ and $[114]_{Al}$ zone axes, where large open, small open and filled circles represent Al, AlSb and Al₂O₃ respectively (c), inverse fast Fourier transformation (IFFT) (d) and FFT (e) images of HRTEM of Al matrix/Al₂O₃(0001) interface taken along Al₂O₃ $[\bar{1}2\bar{1}0]$ axis, and schematic index of FFT image, where open and filled circles represent Al and Al₂O₃ respectively (f)

illustrated in schematic image, it can be deduced that $(0003)_S$ is parallel to $(1\,\overline{1}1)_{AlSb}$ while the $(1\,\overline{1}1)_{AlSb}$ plane is approximately parallel to $(3\,\overline{1}1)_{Al}$ with a tilt about 8° since the diffraction spot $(3\,\overline{1}1)_{Al}$ deviates from $(0003)_S$, as indicated in Fig. 5(c). Therefore, an OR among the substrate, compound AlSb and Al matrix can be concluded as $(0003)_S[\overline{1}100]_S /\!/(1\,\overline{1}1)_{AlSb}[\overline{1}12]_{AlSb} \sim /\!/(3\,\overline{1}1)_{Al}[114]_{Al}$.

As Al matrix solidified at first and then the AlSb phase, the inverse fast Fourier transformation (IFFT) and FFT images were further investigated by the HRTEM of Al matrix/Al₂O₃(0001) interface, which are shown in Figs. 5(d) and (e) along Al_2O_3 [$\overline{12}\overline{10}$] axis. The schematic index of the FFT image is shown in Fig. 5(f). There are two sets of diffraction spots in Fig. 5(f), one set from Al matrix and the other from Al₂O₃, indicating the incident electron beam parallel to $[\overline{12}\,\overline{10}]_S$ axis of Al_2O_3 and [114] axis of Al matrix at the same time. The corresponding planes of Al matrix and Al₂O₃ are labelled in Figs. 5(d) and (f). It is seen that $(000\overline{6})$ plane of Al₂O₃ is parallel to the interface, while (220) plane of Al deviates from the interface with an angle about 26°. The matching directions are [1210]_s // $[\overline{1}14]_{Al}$ and the matching planes at the interface are $(000\overline{6})_{S}$ and $(\overline{220})_{Al}$ but with a 26° tilting angle.

3.4 Lattice parameter and lattice misfit of different nucleated systems

According to the value of 2θ and diffraction spots in XRD and SAED patterns, the *d*-spacing of different crystal planes for Al and Al–Sb solid solution can be calculated and listed in Table 1. The "+" and "–" represent that experimental *d*-spacings of Al and Al–Sb solid solution are extended and compressed, respectively, compared with the referenced value d_0 [28].

Table 1 *d*-spacings of different crystal planes for Al and Al–Sb solid solution combined with referenced value d_0 [28]

(hlk)	d_0 /Å	Al		Al-1%Sb	
		$d_{ m XRD}$ /Å	$d_{ m SAED}$ /Å	$d_{ m XRD}/{ m \AA}$	$d_{ m SAED}/{ m \AA}$
{111}	2.3381	+2.3385		+2.3400	
{200}	2.0248	+2.0256	+2.0296, -2.0190	+2.0266	
{220}	1.4318	+1.4320		-1.4293	-1.4180
{311}	1.2210	+1.2212		1.2210	+1.2240

For pure Al, $d_{(0\overline{2}0)}$ from SAED is extended to 2.0296 Å and $d_{(\overline{2}00)}$ is compressed to 2.0190 Å. That is because two sets of planes $(0\overline{2}0)_{\rm Al}$ and $(11\overline{2}0)_{{\rm Al}_2{\rm O}_3}$ intersect at the interface and $d_{(11\overline{2}0)}$ is larger than

 $d_{(0\overline{2}0)}$ at the matching direction, which places the Al crystal under tensile stress. While all d-spacings from the XRD are extended a little, with the lattice expansion at high temperature and an average of {200} at different directions. For Al-Sb solid solution, $d_{(\overline{220})}$ from the SAED is reduced to 1.4180 Å and $d_{(3\overline{1}1)}$ is increased to 1.2240 Å. Furthermore, $d_{\{220\}}$ from the XRD pattern is also decreased to 1.4293 Å, compared with the referenced d_0 . It is indicated that the contribution of Sb solution in Al to the decrease in {220} planes exceeds lattice expansion at high temperature and an average of {220} at different directions. The lattice parameter for Al and Al-Sb solution at the nucleation interface is calculated as 4.0590, 4.0380 and 4.0107 Å, respectively, based on interplanar spacing $d_{(0\overline{2}0)}$, $d_{(\overline{2}00)}$ and $d_{\{220\}}$ from SAED patterns.

Based on the data available in HRTEM and SAED patterns, the two-dimensional planar misfit (*f*) between nucleated crystals and substrate can be calculated using the modified Bramfitt equation [25]:

$$f_{(hkl)_{n}}^{(hkl)_{s}} = \sum_{i=1}^{3} \frac{|d_{[uvw]_{s}^{i}} \cos \theta - d_{[uvw]_{n}^{i}}|}{3d_{[uvw]_{n}^{i}}} \times 100\%$$
 (1)

where $d_{[uvw]_s}$ and $d_{[uvw]_n}$ are the interatomic spacings along direction $[uvw]_s$ and $[uvw]_n$; θ is the angle between $[uvw]_s$ and $[uvw]_n$; the subscripts "s" and "n" stand for substrate and nucleated crystal, respectively. It should be noted that planes of $(hkl)_s$ and $(hkl)_n$ used in this work are (0001) plane of Al_2O_3 and the preferred growth plane of newly nucleated phase in XRD pattern, and $[uvw]_s$ and $[uvw]_n$ are low index directions in these two planes.

For Al/Al₂O₃ system, the OR between Al and Al₂O₃ is $(000\overline{3})_S$ $[\overline{1}100]_S$ ~// $(\overline{2}00)_{Al}$ $[001]_{Al}$. Reconstructing interface matching between $(\overline{2}00)_{Al}$ and $(000\overline{3})_S$, it is easy to find the optimal planar matching units. Figure 6(a) shows the atomic arrangement for the interface matching of $(\overline{2}00)_{Al}$ on $(000\overline{3})_S$ schematically with the zone axis of $[00\overline{1}]_{Al}$ parallel to that of $[\overline{1}100]_S$, leaving out the effect of the small tilt between the parallel planes. It is seen that a selected unit cell along $[00\overline{1}]_{Al}$ and $[010]_{Al}$ directions of Al crystal badly matches with a unit cell of Al₂O₃ along $[\overline{2}110]_S$ and $[11\overline{2}0]_S$ of low index directions with a misfit of 16.4%.

Considering the solidification sequence of the Al-1%Sb alloy, where Al matrix will solidify first, the nucleation interface of Al–1%Sb/Al₂O₃ system will be $(\overline{220})_{Al}/(000\overline{6})_{Al_2O_3}$ with XRD and HRTEM analysis. By reconstructing $(\overline{220})_{Al}/(000\overline{6})_{Al_2O_3}$ interface matching with the zone axis of $[00\overline{1}]_{Al}$ parallel to that of $[\overline{12}\overline{10}]_S$ and a tilt 26° between $(\overline{220})_{Al}$ and $(000\overline{6})_{Al_2O_3}$, as shown in Fig. 6(b), an optimal misfit 7.0% between this interface can be obtained when a unit

cell along $[\overline{1}2\,\overline{1}0]_S$ and $[\overline{2}110]_S$ directions of Al_2O_3 matches a unit cell from the bottom planes along $[\overline{1}14]_{Al}$ and $[1\,\overline{1}2]_{Al}$ of Al crystal well. An decrease of lattice misfit from 16.4% to 7.0% may occur when nucleation of Al liquid with addition of Sb on $Al_2O_3(0001)$ substrate.

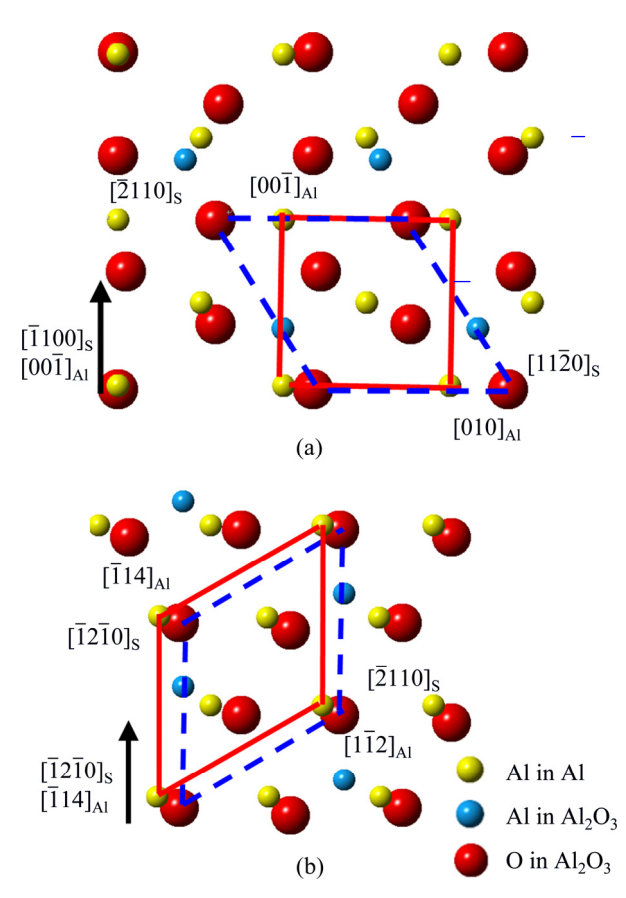


Fig. 6 Schematic illustration of interface matching between $(\overline{2}00)_{Al}$ and $(000\overline{3})_{Al_2O_3}$ (a) and $(\overline{2}\overline{2}0)_{Al}$ and $(000\overline{6})_{Al_2O_3}$ (b)

Therefore, the solution of Sb in Al results in the change of lattice parameter, the crystal orientation and even the lattice misfit of Al matrix crystals nucleated on the $Al_2O_3(0001)$ substrate. Better nucleation efficiency and finer grains can be achieved as a result of the small lattice misfit after Sb turning the lattice structure of Al when it nucleated on the Al_2O_3 substrate.

4 Conclusions

- 1) The preferred crystal orientation of pure Al and Al-1%Sb alloy adjacent to the nucleation interface was examined as (200) and (220), respectively. Small AlSb compounds were identified either at the interface or in the Al matrix of Al-1%Sb alloy by XRD, SEM and TEM in combination with EDS and SADP analysis.
- 2) The evaluation by lattice matching model and the ORs determination by HRTEM confirm that alloy

element Sb enhanced nucleation efficiency and refined grains of Al–1%Sb alloy through the reduced interplanar spacing of preferred orientation and tuned lattice misfit in Al–1%Sb/Al₂O₃ nucleation couple compared with Al/Al₂O₃ nucleation system.

References

- FAHRENHEIT D G. The experiments and observations of supercooled water in vacuum [J]. Philosophical Transactions of The Royal Society, 1724, 33: 78–84.
- [2] MA Qian. Heterogeneous nucleation on potent spherical substrates during solidification [J]. Acta Materialia, 2007, 55: 943–953.
- [3] BUTA D, ASTA M, HOYT J J. Atomistic simulation study of the structure and dynamics of a faceted crystal-melt interface [J]. Physical Review E, 2008, 78(3): 031605.
- [4] KANG J, ZHU Jun-yi, CURTIS C, BLAKE D, GLATZMAIER G, KIM Y H, SU H W. Atomically abrupt liquid-oxide interface stabilized by self-regulated interfacial defects: The case of Al/Al₂O₃ interfaces [J]. Physical Review Letters, 2012, 108(22): 226105.
- [5] OH S H, KAUFFMANN Y, SCHEU C, KAPLAN W D, RÜHLE M. Ordered liquid aluminum at the interface with sapphire [J]. Science, 2005, 310(5748): 661–663.
- [6] BARAM M, GAROFALINI S H, KAPLAN W D. Order in nanometer thick intergranular films at Au-sapphire interfaces [J]. Acta Materialia, 2011, 59(14): 5710–5715.
- [7] LEE S B, KIM Y M. Direct observation of in-plane ordering in the liquid at a liquid Al/α - $Al_2O_3(\overline{1}_10\overline{2})$ interface [J]. Acta Materialia, 2011, 59(4): 1383–1388.
- [8] GANDMAN M, KAUFFMANN Y, KOCH C T, KAPLAN W D. Direct quantification of ordering at a solid-liquid interface using aberration corrected transmission electron microscopy [J]. Physical Review Letters, 2013, 110: 086106.
- [9] NARAYAN J. Recent progress in thin film epitaxy across the misfit scale [J]. Acta Materialia, 2013, 61: 2703–2724.
- [10] WANG L, YANG L, ZHANG D, XIA M, WANG Y, LI J G. The role of lattice misfit on heterogeneous nucleation of pure aluminum [J]. Metallurgical and Materials Transactions A, 2016, 47: 5012–5022.
- [11] WANG Xue-jiao, XU Cong, MUHAMMAD A, HANADA S, YAMAGATA H, WANG Wen-hong, MA Chao-li. Effects of Al-Ti-B-RE grain refiner on microstructure and mechanical properties of Al-7.0Si-0.55Mg alloy [J]. Transactions of Nonferrous Metals Society of China, 2014, 24: 2244-2250.
- [12] FAN Z, WANG Y, ZHANG Y, QIN T, ZHOU X R, THOMPSON G E, PENNYCOOK T, HASHIMOTO T. Grain refining mechanism in the Al/Al–Ti–B system [J]. Acta Materialia, 2015, 84: 292–304.
- [13] LIU Xiao-teng, HAO Hai, ZHU Xiao-xu, ZHANG Xing-guo. Grain refining effect of Mg by novel particle cluster-containing Al-Ti-C master alloy [J]. Transactions of Nonferrous Metals Society of China, 2015. 25: 1804–1810.
- [14] LI Chong, WU Yu-ying, LI Hui, LIU Xiang-fa. Microstructural formation in hypereutectic Al-Mg₂Si with extra Si [J]. Journal of Alloys and Compounds, 2009, 477(1-2): 212-216.

- [15] QIU Ke, WANG Ri-chu, PENG Chao-qun, WANG Nai-guang, CAI Zhi-yong, ZHANG Chun. Effects of Mn and Sn on microstructure of Al-7Si-Mg alloy modified by Sr and Al-5Ti-B [J]. Transactions of Nonferrous Metals Society of China, 2015, 25: 3546-3552.
- [16] QIU Ke, WANG Ri-chu, PENG Chao-qun, WANG Nai-guang, CAI Zhi-yong, ZHANG Chun. Effect of individual and combined additions of Al-5Ti-B, Mn and Sn on sliding wear behavior of A356 alloy [J]. Transactions of Nonferrous Metals Society of China, 2015, 25: 3886-3892.
- [17] LI J H, WANG X D, LUDWIG T H, TSUNEKAWA Y, ARNBERG L, JIANG J Z, SCHUMACHER P. Modification of eutectic Si in Al–Si alloys with Eu addition [J]. Acta Materialia, 2015, 84: 153–163.
- [18] LI J H, HAGE F, WIESSNER M, ROMANER L, SCHEIBER D, SARTORY B, RAMASSE Q, SCHUMACHER P. The roles of Eu during the growth of eutectic Si in Al-Si alloys [J]. Scientific Reports, 2015, 13802: 1-10.
- [19] GOU Jun, TANG Ai-tao, PAN Fu-sheng, SHE Jia, LUO Su-qin, YE Jun-hua, SHI Da-wei, RASHAD M. Influence of Sn addition on mechanical properties of gas tungsten arc welded AM60 Mg alloy sheets [J]. Transactions of Nonferrous Metals Society of China, 2016, 26: 2051–2057.
- [20] REN Bo, LIU Zhong-xia, ZHAO Rui-feng, ZHANG Tian-qing, LIU Zhi-yong, WANG Ming-xing, WENG Yong-gang. Effect of Sb on microstructure and mechanical properties of Mg₂Si/Al-Si composites [J]. Transactions of Nonferrous Metals Society of China, 2010, 20: 1367–1373.
- [21] UZUN O, YILMAZ F, KÖLEMEN U, BASMAN N. Sb effect on micro structural and mechanical properties of rapidly solidified Al–12Si alloy [J]. Journal of Alloys and Compounds, 2011, 509: 21–26.
- [22] WANG Li-ping, CAO Guo-jian, ZHANG Jian-jiao, WANG Guo-jun, LÜ Xin-yu, GUO Er-jun. Effect of combined RE-Ba-Sb addition on microstructure and mechanical properties of 4004 aluminum alloy [J]. Transactions of Nonferrous Metals Society of China, 2013, 23: 2236-2242.
- [23] FARAHANY S, OURDJINI A, BAKHSHESHI-RAD H R. Microstructure, mechanical properties and corrosion behavior of Al-Si-Cu-Zn-X (X=Bi, Sb, Sr) die cast alloy [J]. Transactions of Nonferrous Metals Society of China, 2016, 26: 28-38.
- [24] WANG Hui-yuan, LIU Feng, CHEN Lei, ZHA Min, LIU Guo-jun, JIANG Qi-chuan. The effect of Sb addition on microstructures and tensile properties of extruded Al–20Mg₂Si–4Cu alloy [J]. Materials Science and Engineering A, 2016, 657: 331–338.
- [25] BRAMFITT B L. The effect of carbide and nitride additions on the heterogeneous nucleation behavior of liquid iron [J]. Metallurgical Transactions, 1970, 1(7): 1987–1995.
- [26] MCALISTER A J. The Al-Sb (aluminum-antimony) system [J]. Bulletin of Alloy Phase Diagrams, 1984, 5(5): 462-465.
- [27] YANG L, XIA M, LI J G. Epitaxial growth in heterogeneous nucleation of pure aluminium [J]. Materials Letters, 2014, 132: 52–54.
- [28] WANG Y, LI Hu-tian, FAN Zhong-yun. Oxidation of aluminium alloy melts and inoculation by oxide particles [J]. Transactions of the Indian Institute of Metals, 2012, 65(6): 653–661.

Al-Sb 合金与单晶 Al₂O₃基底的形核界面

王 璐 1,2, 杨 林 2, 张 迪 1, 夏明许 1, Yun WANG 3, 陈 彬 1, 李建国 1

- 1. 上海交通大学 材料科学与工程学院, 上海 200240;
 - 2. 江苏理工学院 材料与工程学院, 常州 213001;
- 3. BCAST, Brunel University, Uxbridge, Middlesex UB8 3PH, UK

摘 要:采用 X 射线衍射、扫描电镜、高分辨透射电镜等分析手段研究了在蓝宝石(0001)基面上异质形核的 AI 合金的晶体取向和界面结构特征。结果表明,在纯 AI 和 AI-1%Sb(质量分数)形核体系中,靠近形核界面处的形核相择优取向分别是 <math>AI 的(200)和(220)晶面,并获得了两种形核体系的位相关系。相比 AI/AI_2O_3 形核体系, $AI-1%Sb/AI_2O_3$ 形核体系中由于合金元素 Sb 的添加,降低了形核相择优生长方向的晶面间距,同时将形核相与形核基底之间的晶格错配度从 AI/AI_2O_3 形核体系的 16.4%降低到 7.0%,因此, $AI-1%Sb/AI_2O_3$ 形核体系具有更好的形核效率和更加细化的晶粒。

关键词: Al 合金; 形核; 界面结构; 位相关系

(Edited by Bing YANG)